Chapter 4. Characteristics of Argon Beam

For efficient beam transport system design, it is important to determine the characteristics of an extracted beam. The beam profile describes the current distribution, beam width and beam angular divergence whereas the beam emittance defines how efficiently it can be transported with minimum loss. The energy spread determines the range of energies of beam ions. This chapter describes diagnostic techniques used for determination of those properties of an extracted Ar beam.

4.1 Experimental Arrangement

The experimental setup used is shown in Fig. 4.1. The ion source is connected to a 250 ls^{-1} turbomolecular pump and powered by a 1.2 kW rf generator via the matching network. The gas supply is controlled by a MKS mass flow controller.

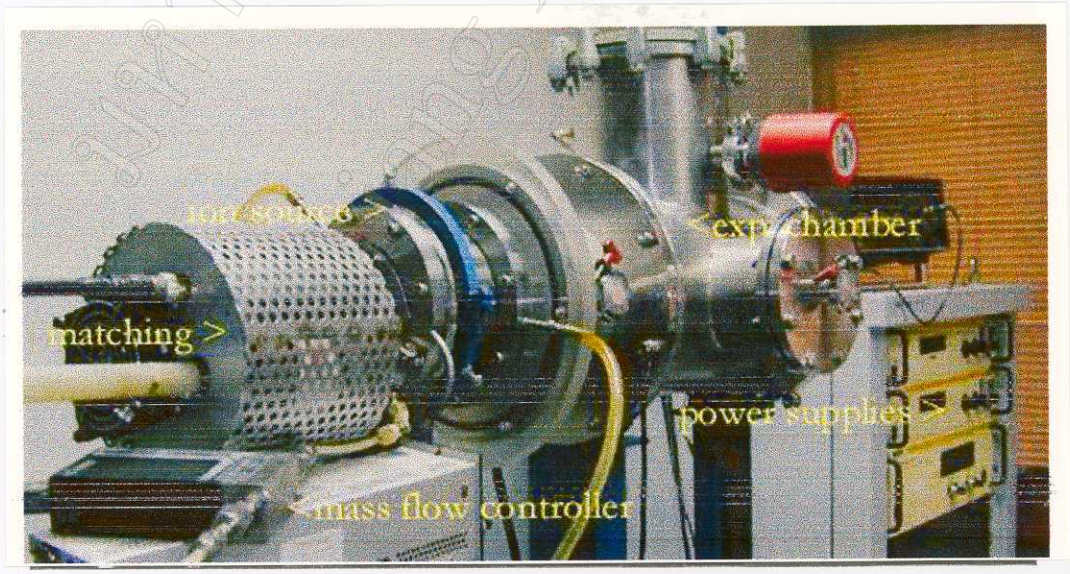

Fig. 4.1 System setup consisted of ion source, experiment chamber, and window

The experiments have been done under these conditions; Argon with flow rate from 0.5 to 5 sccm for operating pressure of 2-45 mTorr and rf power between 0-500 watts unless otherwise specified. The rf power was kept maximum at 500 watts to prevent antenna overheat in a long cw mode operation.

The normal operation residual gas pressure was about 2-3x10^{-6} Torr. The power supplies for extraction, electron suppression, electrostatic lens and retarding field electrodes were mounted in a standard 19 inch rack for easy operation and shielded from the rf interference. Measuring devices such as, vacuum gauge, multimeter, PC and etc. were also kept far away from the source area to prevent rf noise. To decouple the rf noise from the extraction voltage, a 1.2 mH rf choke was inserted in series with the dc high voltage supply. This inductor with small stray capacitance functions as a simple L-C low pass filter. The antenna leg between antenna and matching network was well shielded and the rf power supply was operated at the extracting potential to reduce rf coupling to the experimental setup.

4.2 3-Electrode Extracting System

We used computer simulations to optimize the electrode geometry. Fig. 4.2 shows a typical example of a simulation by program KOBRA3-INP (Spadtke, 1999) of a 9 keV Ar beam extracted from a triode extraction system after calculation described in section 2.3. The code KOBRA3-INP, which uses Finite Difference Method (FDM), includes the solution of the Poisson equation and particle distribution function in 3 dimensions. It creates the space charge map during the ray-tracing which give an exact beam trajectories result. This 32-bit version running under extended DOS needs over 128 MB memory on a fast PC

for better performance. Argon current density was defined as 25 mA/cm^2 for the whole simulation.

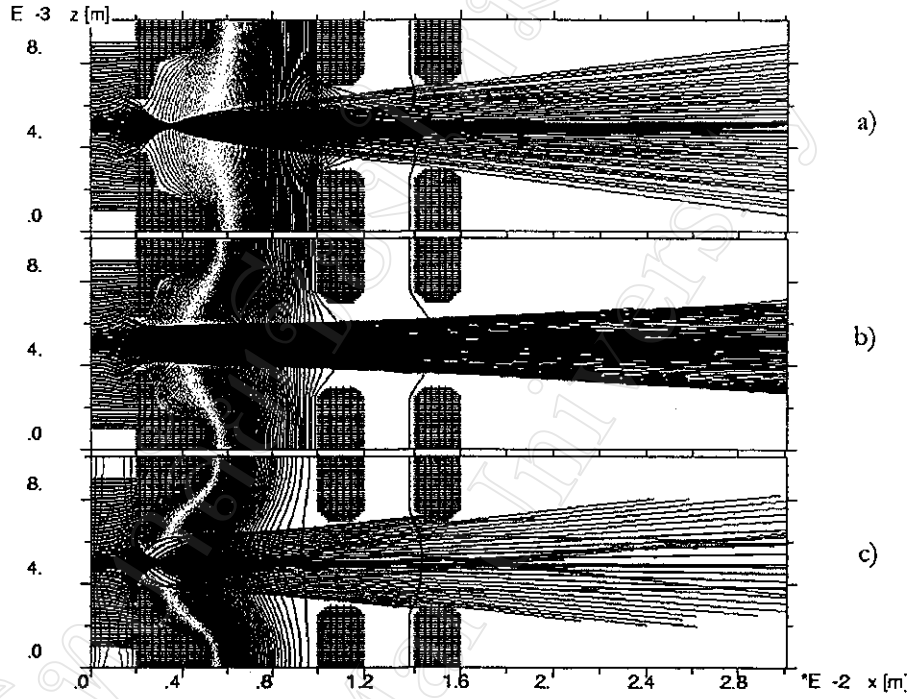

Fig. 4.2 Samples of KOBRA simulation of 9 keV Ar beam from a 3 electrode extraction system at different values of perveance a) $0.3P_0$, b) $0.45P_0$ and c) $1.0P_0$. The grids were biased with 9, -1 and 0 kV, respectively. Note: $P_0 \approx 1.2\text{x}10^{-9}$ A/V$^{3/2}$

The perveance is varied to see its influence on beam optics. It can be observed that for a beam perveance greater or less than 0.45 the beam diverges and is not uniform. The beam in Fig. 4.2(b) has a minimum emittance of about 29 mm mrad (described in section 4.4). For the simulation, ion temperature was assumed to be 0.1 eV instead of zero to see its effect on beam divergence at low energy extraction. Fig. 4.3 shows an Ar beam current extracted from the source as a function of Argon pressure. It indicates the

optimum operating pressure for this type of discharge, chamber size and rf frequency (Engemann, 2001). In other words, the peak pressure for maximum discharge efficiency for this geometry and rf frequency is around 8 mTorr. Table 4.1 compare gas and electron ionization mean free paths of Argon at 300 K. It can be seen that the ionization mean free path is the same order of the source chamber (10 cm) at Argon pressure of about 10 mTorr. This result is also in agreement with the OES result in Fig. 3.7 c) where Ar ions decrease as increasing of the gas pressure over 10 mTorr even though the ionization mean free path becomes shorter. However the gas mean free path also reduces leads to fall of ionization efficiency at high pressure (electrons need a distance of 2.4 cm to reach 11 eV kinetic energy in 13.56 MHz field (Chapman, 1980)). This value of pressure was used throughout the whole measurement.

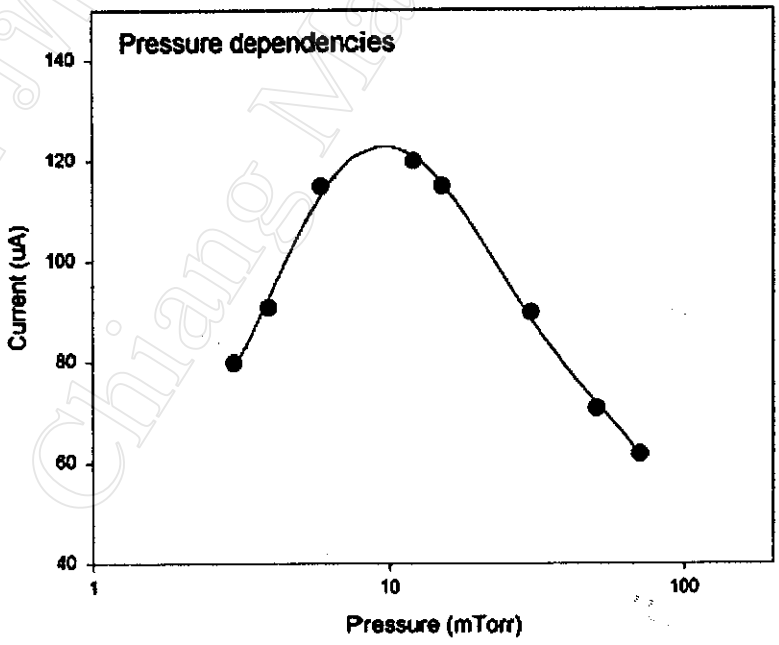

Fig .4.3 Pressure dependencies of the extracted Ar beam from this setup

Table 4.1 Comparison of gas and ionization mean free path at various Argon pressures (n is number of density = $3.2\times10^{22}P$ (Torr) m^{-3}, d is atom diameter and σ_{iz} is ionization cross section (see Fig. 2.1)).

Argon pressure (mTorr)	Gas mean free path $\lambda \approx 0.707/n\pi d^2$ (cm)	Ionization mean free path $\lambda = 1/n\sigma_{iz}$ (cm)
1	4	80
10	0.4	8
100	0.04	0.8

To determine an extractable current from the ion source, Ar beam was extracted from a 1 mm diam beam exit at different rf powers. The faraday cup current plotted against the extracting voltage at a base pressure of 8 mTorr, is shown in Fig. 4.4. It can be seen the current increase with extracting voltage and become saturated at different higher extracting voltage. The left-hand side of the rising curve corresponds to a voltage-limited extraction regime where the extracted current, for a given geometry, is set by the extracting voltage, as described by the Child-Langmuir law discussed in the previous chapter. This is analogous to the space charge-limited operation mode of a diode. As the extracting voltage is increased further, the extracted current saturates. In other words, the right-hand side of the rising curve corresponds to an emission-limited regime, in which the extraction of all available current is reached. By measuring these saturated currents, the maximum current density for the ion source at different rf power can be determined. Compared with previous measurement (Boonyawan et al,1999), the current density of Argon increases from 29 mA/cm^2 to 36 mA/cm^2at 500 watts rf power. Even though there is no

significant difference in the field free region of those sources using different type of permanent magnets as indicated in Fig. 2.4.

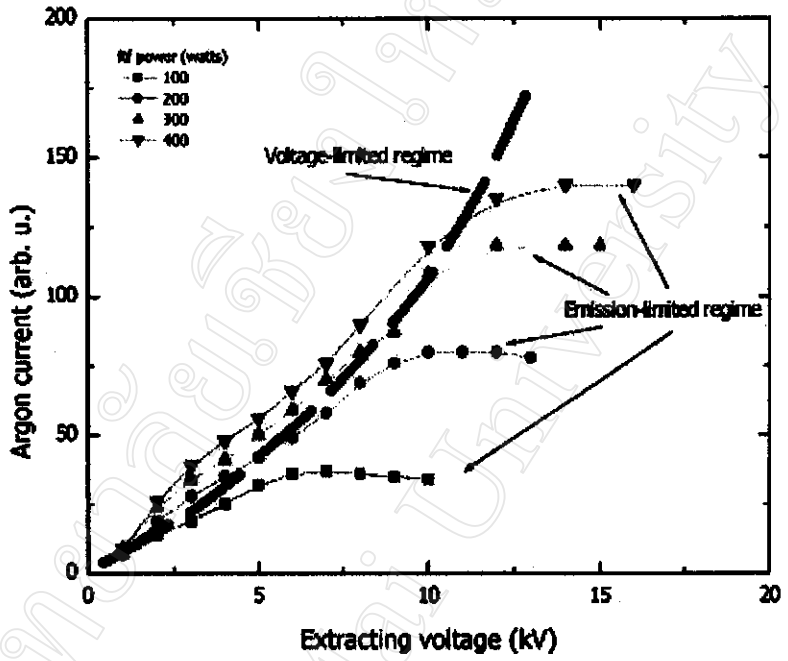

Fig. 4.4 Ar current extracted from the ion source at different rf power at a base pressure of 8 mTorr.

Another factor that can be determined from this result is α, the ratio of an extractable current density J_i to a producible current density $ne(kT_e/m_i)^{1/2}$ where n is the plasma density measured by the Langmuir probe in section 3.4. It is found that α is equal to 0.59 ± 0.1 which agrees with the result measured by Suanpoot et al (1998). This ratio is independent of the driving rf power (Forrester, 1988).

4.3 Scanning Wire Beam Profile Monitor

A beam profile monitor (BPM) consists of a simple sensing wire working as a beam current sensor, a motorized stage and an analog to digital converter

(ADC). If the Ar beam energy is much below 2 MeV/u, then Ar will be stopped completely in the wire and a current signal is then generated from those collected ions. The current flows through a small value resistor, it generates a voltage peak for an ADC. The wire has to be moved continuously by a fine stepping motor. The collected voltage values are then interfaced and displayed on the PC as the voltage profile.

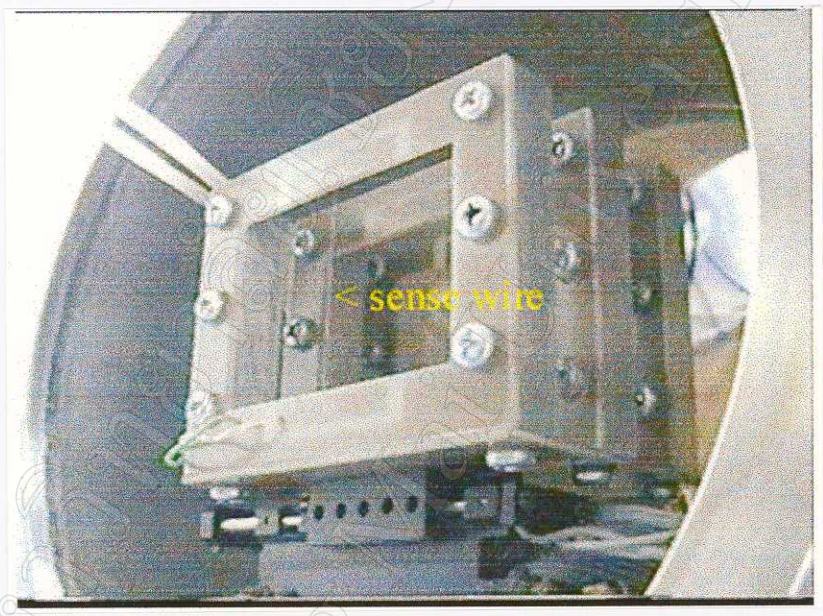

Fig. 4.5 Show 50 micron W wire as a beam sensor on scanning wire BPM

Fig. 4.5 shows the three 50 micron sensing wires (Tungsten) stretched in PCB frames which were separated by 2 cm each in the down stream direction. The frames sit on a miniature motorized stage inside the vacuum chamber. The beam currents are collected by a Universal Serial Bus (USB) data acquisition system model OMEGA OMB-DAQ-55. The stage is controlled by a single axis intelligent drive model MicroMini^{TM} controller via RS-485 interface with 2.5 cm maximum scan range. The stage resolution is better than 0.5 μm so the systematic profile resolution is equal to 50 micron which is about the diameter of

the sensing wire. The secondary electrons suppression was done by bias the sense wire with a positive voltage. The plateau of the bias voltage depends slightly on beam energy as shown in Fig. 4.6. However it is found that the measured profile is not depending on the bias voltage and, especially, there is no neighboring wires which can generate electrons to distort the profile (Strehl, 1995).

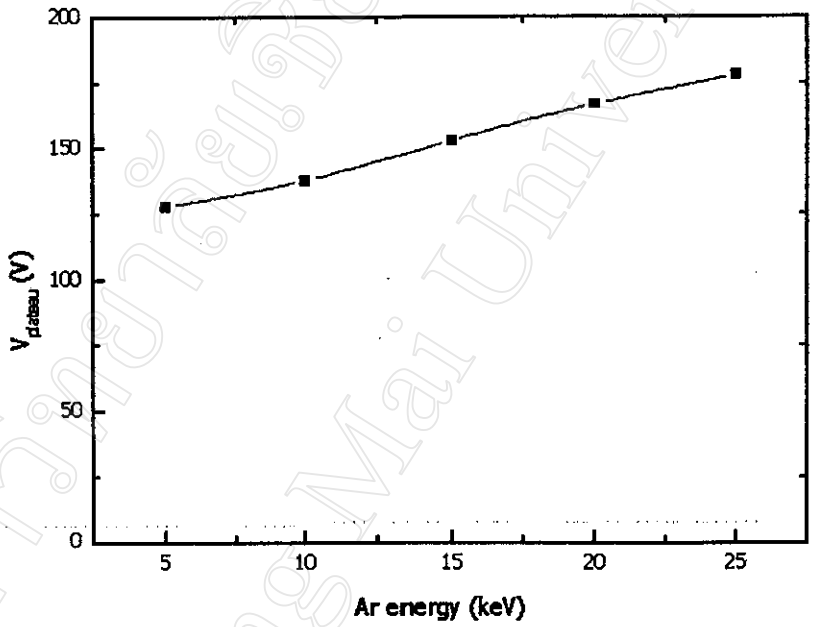

Fig. 4.6 Plateau of the bias voltages plot as a function of Ar beam energy

The beam profile can be displayed, stored and analyzed by a program developed in Microsoft Visual Basic which also includes the controller routine to control the scanner, detects and resets the limiting switch. Fig. 4.7 shows the beam profiles at a distance of 3 cm from the ground electrode of the ion source. An increase in extracting voltage decreases the beam width and divergence angle. The velocity of the emitted ion from the plasma has both axial and transverse components. The axial component is proportional to the extracting

energy (eV) while the transverse component is proportional to the ion transverse kinetic energy (kT_i) which causes the spread of the beam width. Therefore, the beam divergence or the so-called source emittance-limited divergence can be written (Zakhary et al, 1995)

$$\theta \propto \sqrt{(kT_i / eV)} \tag{4.1}$$

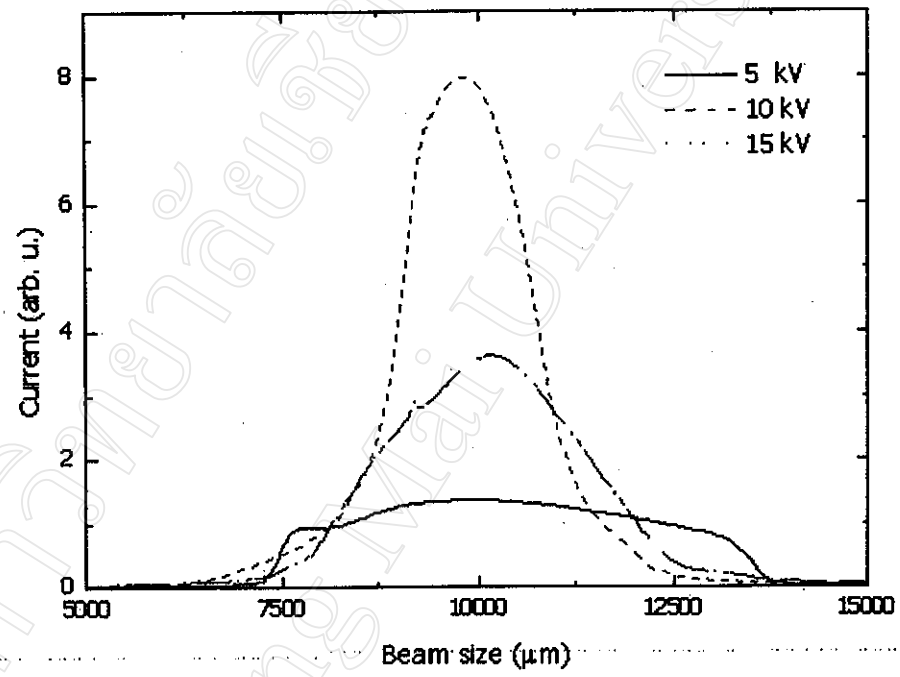

Fig. 4.7 A measured beam profile as a function of the extracting voltage at 3 cm from the ground electrode using the scanning wire BPM

To test the scanning wire BPM resolution, the 1 mm Ar beam is focused by an Einzel lens installed upstream closed to the ion source. The lens voltage is set to 7 kV. It can be seen in Fig. 4.8 that the focusing effect started on the first (left), fully focused on the middle and again diverged on the third (right) wire. The full width at half maximum (FWHM) of the beam profile was 250 micron at fully focused and the peak current was about 16 μA (no suppression).

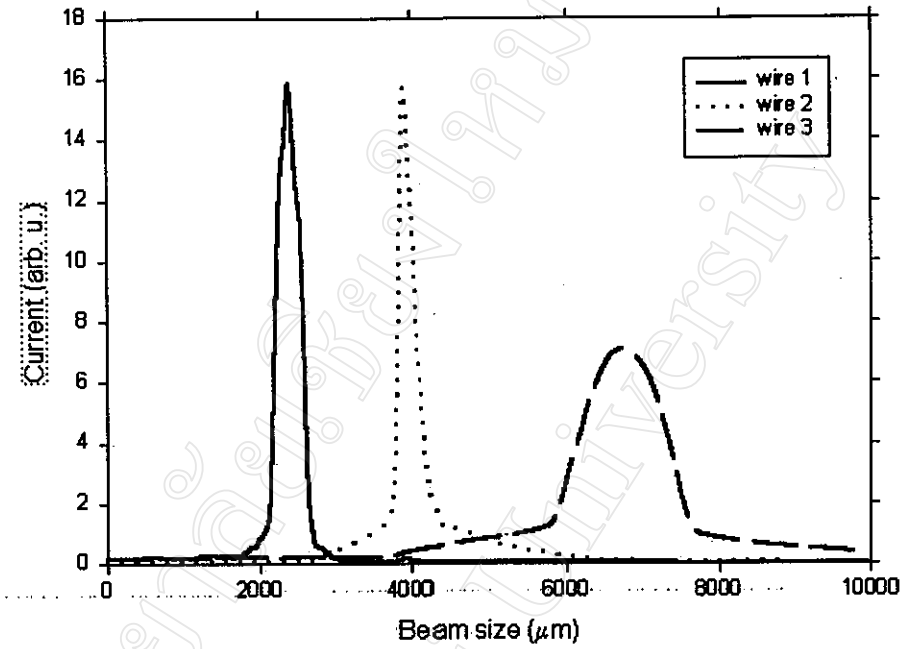

Fig. 4.8 The beam profile of the 12 keV focused Ar beam at different locations.

4.4 Beam Emittance Measurement

The beam emittance diagram from an ion source is an essential property for beam transport system design. To avoid complicated hardwares and destructive properties in many beam emittance measurement devices, a quadrupole scan method has been adopted. The method requires only a quadrupole followed by a beam profile monitor. To briefly describe the method, consider a beam phase space diagram as shown in Fig. 4.9 and the definition of the beam matrix (Strehl, 1995).

$$\sigma = \begin{bmatrix} \sigma_{11} & \sigma_{12} \\ \sigma_{21} & \sigma_{22} \end{bmatrix} = \varepsilon \begin{bmatrix} \beta & -\alpha \\ -\alpha & \gamma \end{bmatrix}, \tag{4.2}$$

where $\beta,\alpha,\gamma,\varepsilon$ are ellipse parameters (see Appendix C), $\alpha = -\beta'$ and $\beta\gamma = (1+\alpha^2)$.

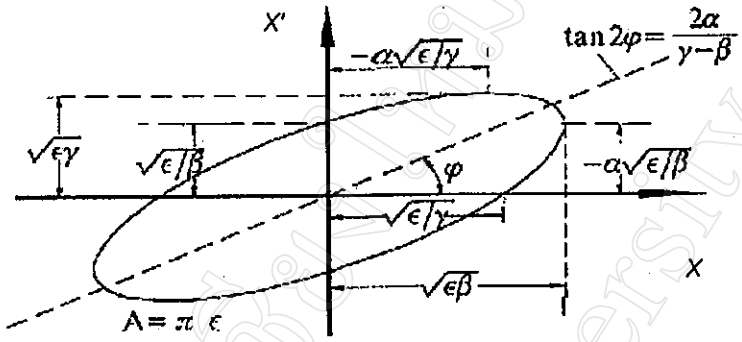

Fig. 4.9 A phase ellipse of a beam in phase space (Wiedemann, 1997)

At different positions along the beam transport line the phase ellipse will change its form and orientation, but not its area. The ellipse parameters at any position down stream from the quadrupole are given by

$$\begin{bmatrix}\beta\\ \alpha\\ \gamma\end{bmatrix} = \begin{bmatrix} c^2 & -2sc & s^2 \\ -cc' & (s'c+sc') & -ss' \\ c'^2 & -2s'c' & s'^2 \end{bmatrix}\begin{bmatrix}\beta_0\\ \alpha_0\\ \gamma_0\end{bmatrix}, \tag{4.3}$$

where $\beta_0,\alpha_0,\gamma_0$ are the ellipse parameters at the entrance of the quadrupole. The transformation matrix elements c, s, c', s' are given by the quadrupole focal length, f and the length L of the drift space between the quadrupole and the beam profile monitor

$$\begin{bmatrix} c & s \\ c' & s' \end{bmatrix} = \begin{bmatrix} 1 & L \\ 0 & 1 \end{bmatrix}\begin{bmatrix} 1 & 0 \\ -1/f & 1 \end{bmatrix} \tag{4.4}$$

Utilizing the definition of the beam matrix in (4.1) and $\sigma_{12} = \sigma_{21}$ one get for the determinant

$$\sigma_{11}\sigma_{22} - \sigma_{12}^{\ 2} = \varepsilon^2, \tag{4.5}$$

and the beam sizes at the beam monitor are given by

$$\sigma_{11,monitor} = s^2\sigma_{11} + 2sc\,\sigma_{12} + s^2\sigma_{22} \quad (4.6)$$

By varying the focal length, we measure $\sigma_{11,monitor}$ as a function of the quadrupole strength, *k*. All parameters in (4.6) are known except for σ_{11}, σ_{12} and σ_{22}. By fitting these parameters to the measured curve $\sigma_{11,monitor}(f)$, the beam emittance ε can be obtained from (4.5). In addition from (4.2) one can also determine the orientation of the phase ellipse. Thus, all parameters $(\beta_0, \alpha_0, \gamma_0, \varepsilon)$ to design a beam transport line are determined

The emittance of the triode extracting system, designed in 4.2, using the quadrupole scan method was obtained with a setup as shown in Fig. 4.10a). It consists of a quadrupole lens (4.10b) and a multiwire beam profile monitor (4.10c). The extracting system includes three stainless-steel electrodes with 8 and 2 mm spacing and a 2.5 mm diam beam exit hole. All edges have been removed to enhance beam quality as reported before by Reijonen et al (1998). A quadrupole (Junphong, 1999) with a 5 cm aperture and a maximum strength of 5.0 Tesla/m was installed 10 cm from the ground electrode. The beam profile was located 20 cm from the quadrupole. A profile monitor originally developed by Godfrey et al (1990) was modified to have a 3x3 cm^2 active area with 16x16, 150 micron Tungsten sense-wires. A 4 cm diam. electron suppressor dish is biased at -200 V. The signals from each sense-wire were read out through external multiplexers to a digital storage oscilloscope for beam width determination.

An Ar beam was extracted at 9 kV with suppression electrode biased at –500 V and 300 W rf power. From the beam width measurement by the beam profile monitor, beam parameters can be derived.

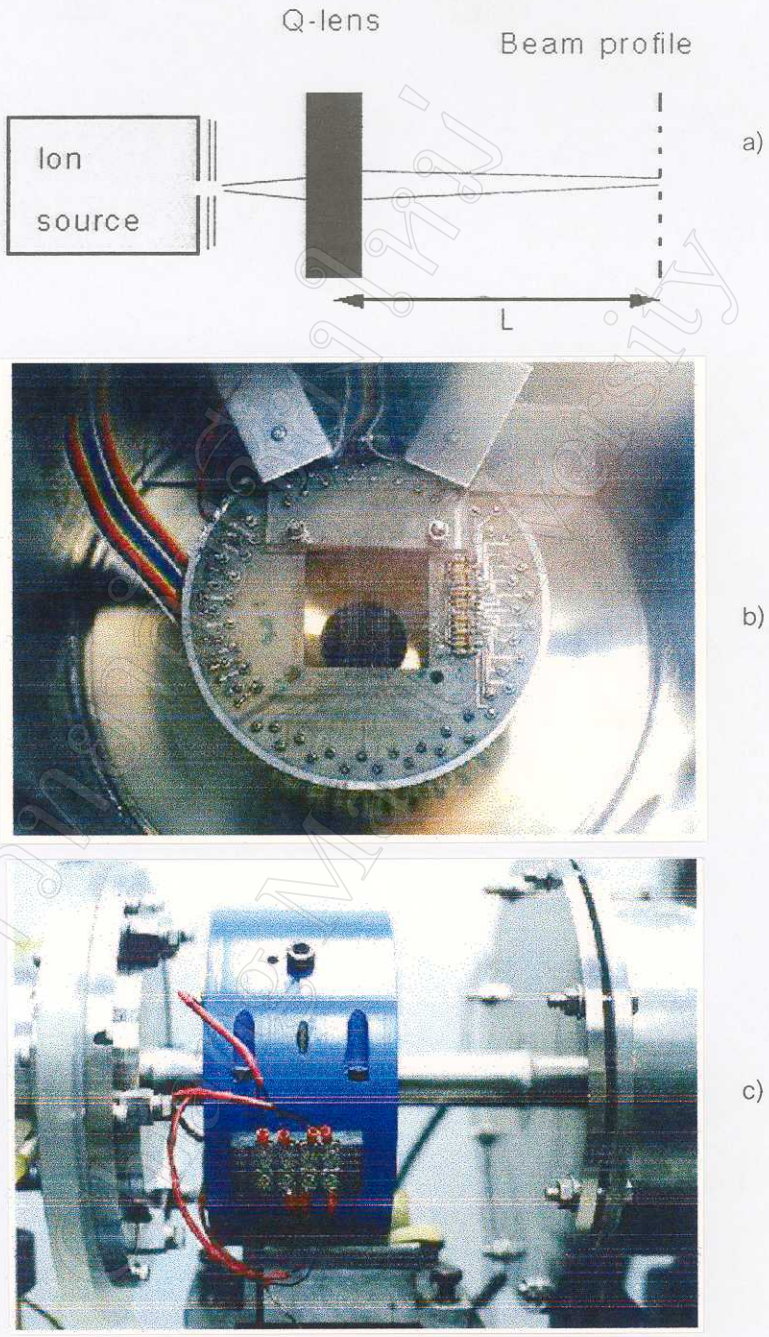

Fig. 4.10 Emittance measurement setup using quadrupole scan method a) schematic diagram b) a quadrupole magnet c) a 16x16 multiwire BPM

Fig. 4.11 shows the polynomial fit of quadrupole current vs beam width. The fitting constants represented the parameters in (4.5). A typical phase space diagram of the emitted beam is then plotted as shown in Fig. 4.12.

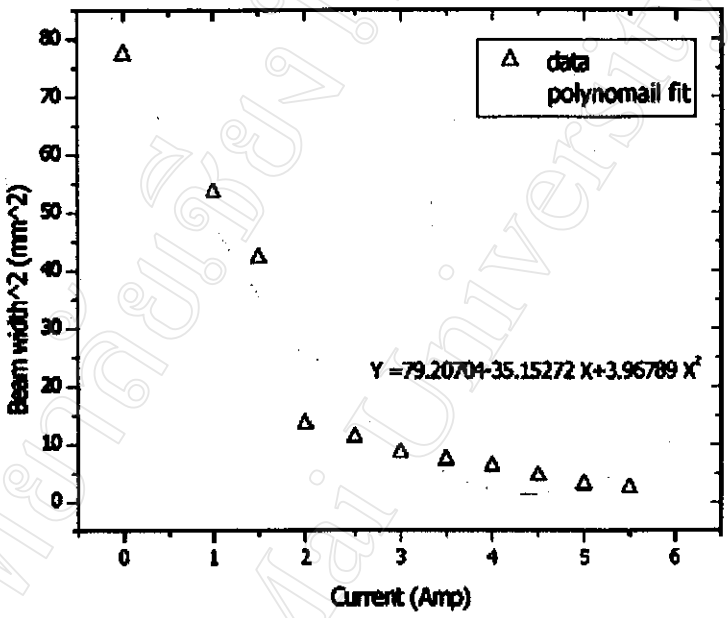

Fig. 4.11 A plot of polynomial fitting between quadrupole current vs beam width

The rms emittance ε = 32 ± 4 mm mrad is consistent with the KOBRA calculations in Fig. 4.3(b). From the calculation, about 86 % of the beam particles are in the phase-space ellipse. These calculations optimize the extracting system for an Argon density varying from 25 to 75 mA cm^{-2} and the rms emittance is found to vary between 28 and 48 mm mrad at 9 kV extraction. Thus measurement also provides information on the beam size, $x = (\varepsilon\beta)^{1/2}$ = 6 mm and the beam divergence, $x' = (\varepsilon\gamma)^{1/2}$ = 12 mrad at the entrance to the quadrupole. The uncertainty in this measurement is mainly due to wire spacing of the beam profile monitor and polynomial fitting. The emittance of this ion

source is fairly small compared to the value of 200-400 mm mrad as measured in an rf ion source by Abdelaziz et al (2000). Expressed in term of normalized rms emittance defined by $\varepsilon_n = (2V/mc^2)^{1/2}\varepsilon$, where V is the accelerating voltage, m is the ion mass, c is the speed of light, it is found to be only 0.02 π mm mrad compared to 0.04 π mm mrad in double electrode extracting system measured by Leung et al (1998) for an Ar beam. It should be noted that Leung et al used a different type of emittance measuring device (electrostatic, slit to slit or Allison type emittance scanner) and a double electrode extracting system. Also, they measured the emittance at higher rf power.

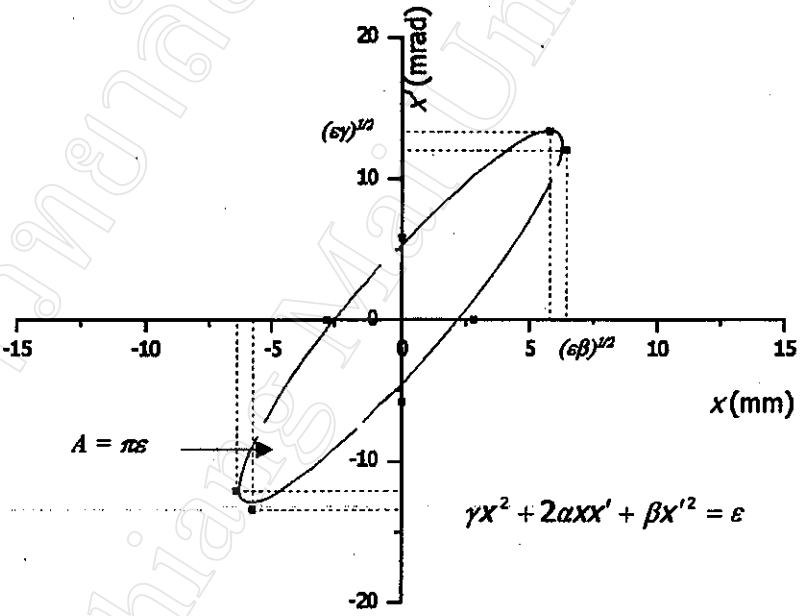

Fig. 4.12 Phase-space diagram of 9 keV Ar beam results the rms beam emittance of 32 ± 4 mm mrad

4.5 Beam Energy Spread Measurement

The energy spread of an accelerated beam was measured by the following procedures. The collected ion current as a function of retarding voltage was first measured and the current-voltage (I-V) curve was then

differentiated and inversely plotted to determine the energy spread (ΔE) which is defined as the full width at half maximum (FWHM) of the differentiated curve. A self-built retarding field energy analyzer (RFA) (Engemann, 2001) has been made for this experiment. The energy spread was measured on an accelerated Ar beam. The assembly is illustrated schematically in fig. 4.13 a). The energy analyzer has a 7 cm long and 3 cm diameter grounded metal shield with a 3 mm inlet aperture defining the incoming beam, an electron suppressor for secondary electron suppression and a collector for energy distribution measurements.

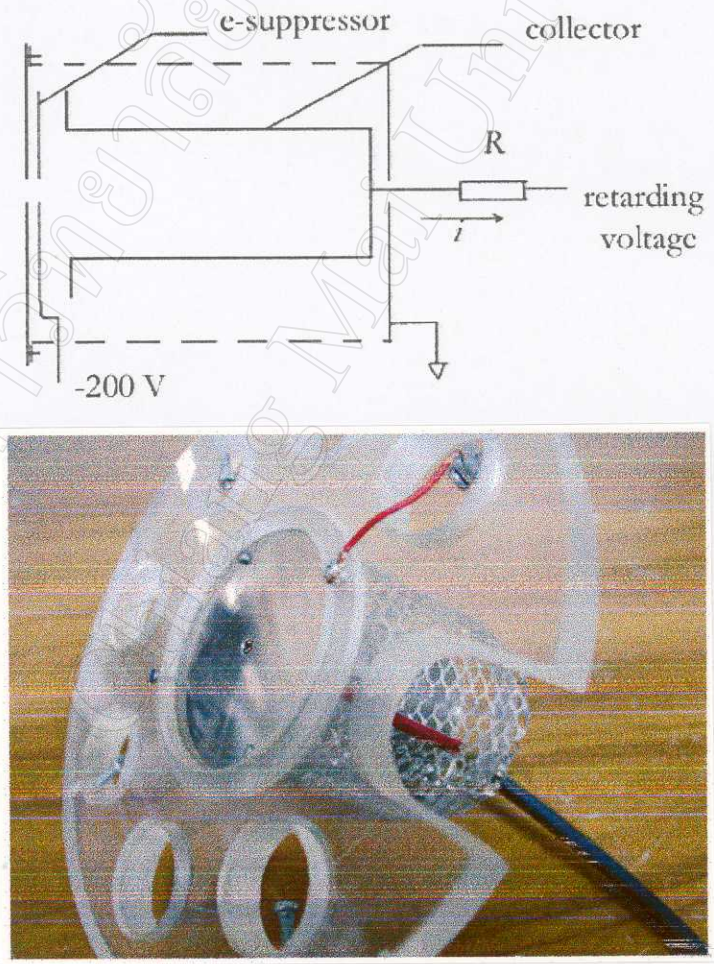

Fig. 4.12 The RFA developed for beam energy spread measurement
a) schematic diagram b) actual RFA with a ground shield

The collector is connected to a retarding voltage via a 100 kΩ resistor which determines the collected current. The analyzer was mounted about 10 cm from the ground electrode of the extraction system. Fig. 4.13 b) shows the actual RFA made from stainless steel, cylindrical in form and attached to a plastic holder for installation to the experiment chamber. The collected current is fed through a shield coaxial cable to prevent rf noise. The secondary electron yield is determined form this RFA and found that at 3 keV Ar beam the yield is about 0.5. The suppressor is then adequately set at -200 V.

At 200 watts rf power and 4 kV extracting voltage, the energy spread is found to be 3.6 ± 0.5 eV at 8 mTorr gas pressure. Measurements indicate that the energy spread depends on the extracting voltage as shown in Fig. 4.14. This voltage dependence has been reported by Kuo et al (1998) and was explained that the space charge effect is reduced as increasing of extracting voltage. The high fluctuation of the energy spread at low extracting voltage may be due to an rf interference and an instability of the dc power supply itself. The measurement became much more stable when the extracting voltage exceeds 2 kV. The energy spread has been found to decrease from 4.8 eV to 3.4 eV as the gas pressure increases to 25 mTorr at 500 V extraction. The variation of the energy spread with gas pressure is attributed to the fall of plasma potential which was observed to decrease from 9 to 7 V when the Argon pressure increases from 8 to 25 mTorr. Fig. 4.15 shows an effect of introducing a 0.1 μF bypass capacitor with the rf choke installed. The added capacitor reduced the beam current. This effect may be explained as a reduction of extracting voltage by a high capacitive load resulting in a reduction of extractable beam current. We note that without an rf choke, the energy spread goes up to 5 eV ±1.5 eV.

The rf choke functions as a low pass filter which is effective in eliminating the modulation of the dc acceleration voltage with rf interference.

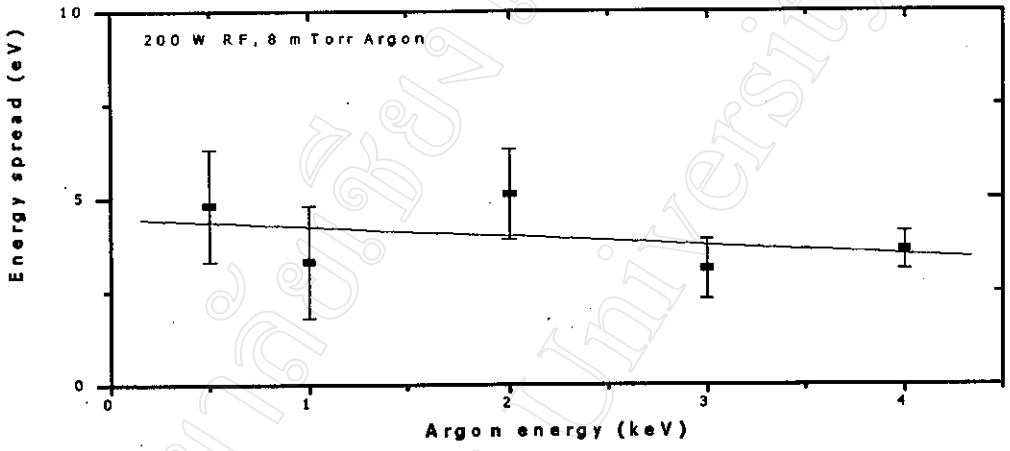

Fig. 4.14 Energy spread of Ar beam at 0.5 to 4 keV energy

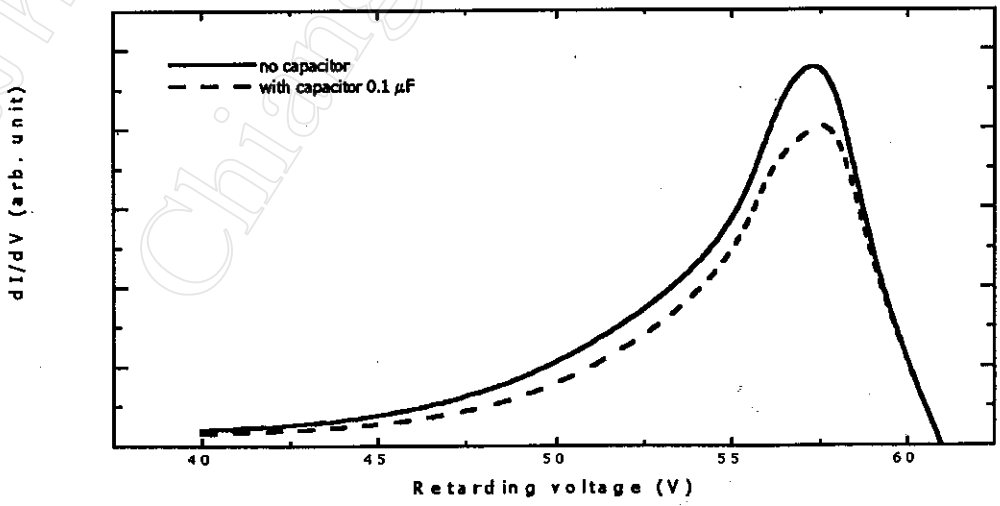

Fig. 4.15 Effects of with and without 0.1 μF bypassing capacitor on energy spread

4.6 FIB System: Conceptual Design Study

In general, an FIB employs a high brightness ion source such as a gas field ionization source (GFIS) or a liquid metal ion source (LMIS). To utilize a plasma source to produce an intense focused ion beam, it is necessary to use multi-aperture extraction. Beams should be parallel with sufficient intensity so the focused beam at the target would be suitably intense. Consider a beam envelope or trajectory equation for an ion beam with radius r_b in free space (Ishikawa, 1998)

$$\frac{d^2 r_b}{dz^2} = \frac{K}{r_b} + \frac{\varepsilon_n^2}{\beta^2 r_b^3}, \tag{4.7}$$

where K is the generalized beam perveance $\equiv I_b / 4\pi V_b^{3/2}\sqrt{2e/m}$ = 6.5 x 10^5 $I_b\sqrt{m}/V_b^{3/2}$, ε_n is the normalized beam emittance = $2r_b\sqrt{kT_i/mc^2}$, β is the ratio of ion speed to speed of light. Equation 4.7 provides information on beam divergence due to space charge (first term) and beam emittance (second term). Table 4.2 compare the effects on a 100 micron Ar beam by using a following ratio of the second term to the first term of (4.7)

$$\alpha = \frac{\varepsilon_n^2 / \beta^2 r_b^2}{K} \tag{4.8}$$

Table 4.2 α ratio as functions of V_b and I_b from a100 micron beam

$V_b(kV)$	$I_b(uA)$	α
1	10	1/6.7
	100	1/67
	1000	1/667
10	10	1/2
	100	1/21
	1000	1/211

It can be seen that beam divergence is dominated by space charge effect. For example, Ar beams from the triode system described in Chapter 3 which have beam divergence of 12 mrad will have α of about 1/10. For the 100 micron beam case from the Table, the 1 keV Ar beam current has to be reduced to 10 μA to minimize space charge effect. In addition, one can also see that an increase of extracting voltage V_b by one order of magnitude will reduce the space charge effect by a factor of 3.

Fig. 4.16 shows a computer modeling of a 1 keV Ar beam extracted from a 100 micron double electrode extracting system at different beam currents. Fig. 4.16(b) is in good agreement with the above calculation that the minimum beam divergence can be achieved when α ratio is close to 1/1. In this case beam emittance as low as 1.1 mm mrad is obtained which implies that the beam divergence of (b) is equal to 25 mrad.

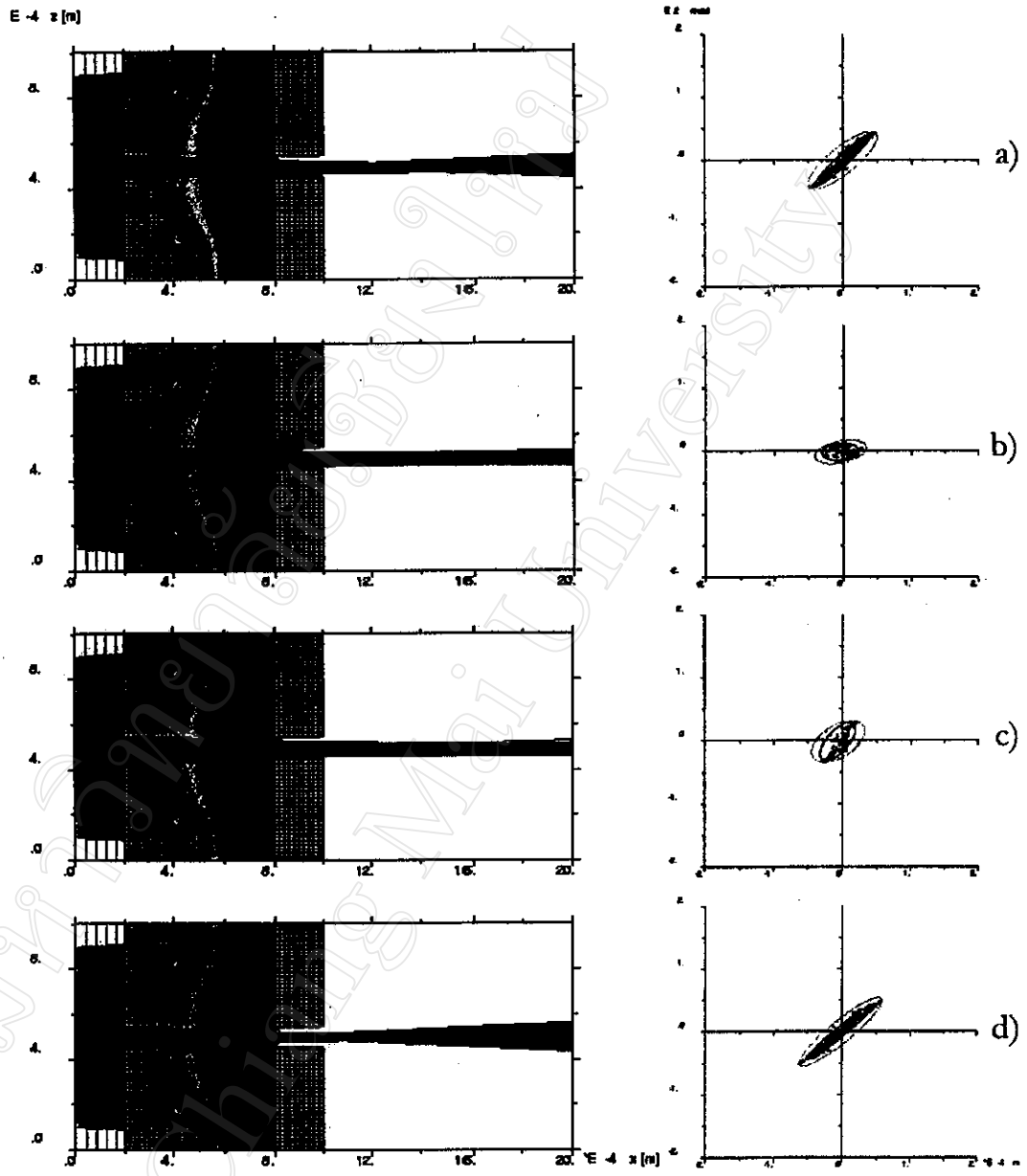

Fig. 4.16 Modeling of the 100 micron beam extraction with its emittance. Ar beam current is extracted with 1 kV for the case of a) 1 μA, b) 10 μA, c) 100 μA and d) 1000 μA

It can be seen from section 4.2 and the above beam modeling that the particular beam will diverge. To overcome this effect in the multi-aperture beam, a simple electrostatic lens can be used to shape the intense beam. The Einzel

lens system consists of three electrodes. The middle electrode is biased to a certain voltage while the two outer ones are grounded. This system performs an accel-decel scheme which focuses the beam without changing its energy. By using KOBRA3-INP we can model an incoming Ar beam of 1 keV, 3 mm diameter with 12 mrad angular divergence passing through an Einzel lens with 6 mm aperture. Fig. 4.17 shows the focusing results at different lens voltage a) 0.5 kV, b) 0.8 kV and c) 1 kV.

It can be seen that a proper lens voltage can focus an incoming beam (b) whereas an over bias causes the beam to diverge strongly (c). Fig. 4.18 is the beam emittance of 0.8 kV case in which beam is fully focused. In addition, Fig. 4.18 also indicates that the output beam emittance is 34 mm mrad which is consistent with the input divergence.

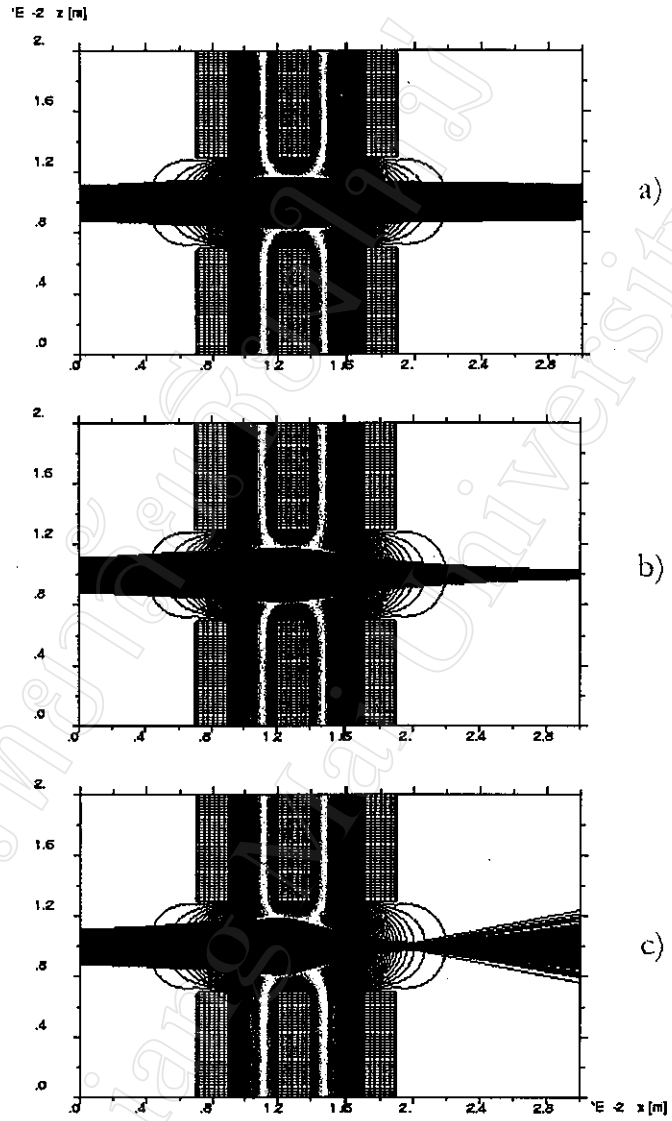

Fig. 4.17 Effects of different lens voltage on the Einzel lens with 6 mm aperture a) 0.5 kV b) 0.8 kV and c) 1 kV

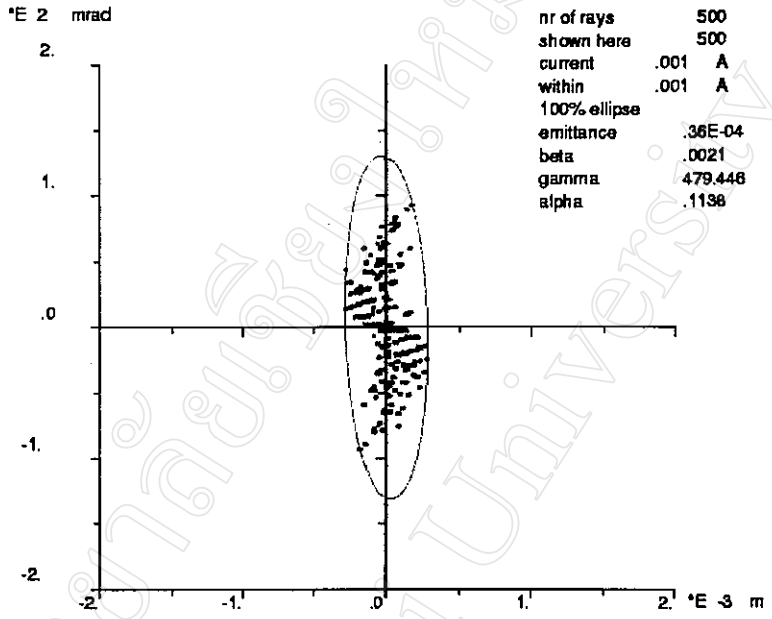

Fig. 4.18 Beam emittance of a 1 keV Ar beam after the 0.8 kV biased Einzel lens